Cancer Immunology, Immunotherapy (2025) 74:164
https://doi.org/10.1007/s00262-025-04017-z

RESEARCH

Multicenter evaluation of predictive clinical and imaging factors for pathological response in non-small cell lung cancer patients treated with neoadjuvant chemotherapy and immune checkpoint inhibitors

Mengzhe Zhang[1] · Meng Yan[2] · Zekun Li[3] · Shuai Jiang[1] · Zuo Liu[1] · Pengpeng Zhang[1] · Zhenfa Zhang[1]

Received: 8 October 2024 / Accepted: 8 March 2025 / Published online: 5 April 2025

Abstract

Background This study aimed to identify clinical factors and develop a predictive model for pathological complete response (pCR) and major pathological response (MPR) in non-small cell lung cancer (NSCLC) patients receiving neoadjuvant chemotherapy combined with immune checkpoint inhibitors (ICIs).

Methods Cases meeting inclusion criteria were divided into high- and low-risk groups according to 75 clinical indicators based on tenfold LASSO selection. Logistic regression was employed to analyze both pCR and MPR. The accuracy of the nomograms was assessed using the time-dependent area under the curve (AUC).

Results A total of 297 patients from four multiple centers were included in the study, with 212 assigned to the training set and 85 to the testing set. The AUC was determined for the prediction of pCR (training: 0.97; testing: 0.88) and MPR (training: 0.98; testing: 0.81). Significant associations were observed between the preoperative tumor maximum diameter, preoperative tumor maximum standardized uptake value (SUV_{max}), changes in tumor SUV_{max}, percentage of tumor reduction, baseline total prostate-specific antigen (TPSA) and pathological response ($P < 0.001$).

Conclusions The combined application of clinical indicators including non-invasive tumor imaging and hematology can help clinicians to obtain a higher ability to predict NSCLC patient's pathological remission, and the effect is better than that of clinical factors alone. These findings could help guide personalized treatment strategies in this patient population.

Mengzhe Zhang, Meng Yan, Zekun Li have contributed equally to this work.

Extended author information available on the last page of the article

Graphical abstract

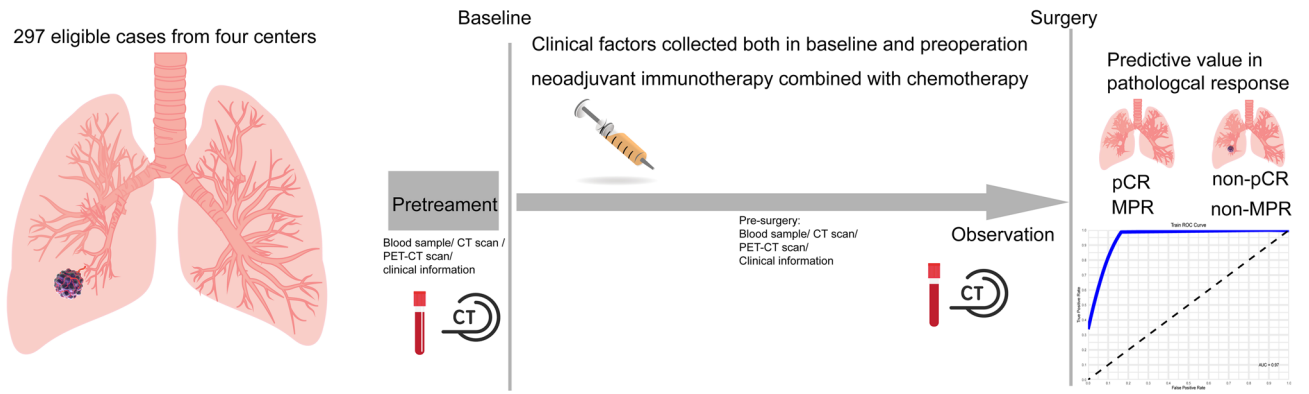

Totally 297 eligible non-small cell lung cancer patients receiving neoadjuvant immunotherapy are divided into training-set and testing-set using clinical factors by LASSO and logistics regression. We compare the pathological response in all sets, significant difference exists.

Keywords Non-small cell lung cancer · Pathological complete response · Major pathological response · Immune checkpoint inhibitors · Prognostic clinical indicators · Tumor imaging biomarkers

Introduction

Lung cancer continues to be the most prevalent malignant neoplasm worldwide [1], with its incidence rising annually [2]. In recent years, immunotherapy has emerged as a promising treatment for patients with non-small cell lung cancer (NSCLC), particularly in chemotherapy-resistant cases [3]. Gene signatures related to inflammation and epithelial–mesenchymal transition have been identified in chemotherapy-refractory NSCLC, offering new insights into treatment response [4]. Identifying molecular markers that can predict patient responses to frontline treatments holds significant potential for advancing personalized therapies, such as immune checkpoint inhibitors, allowing targeted interventions for those most likely to benefit [5].

Although pathological complete response (pCR) is considered the optimal endpoint for neoadjuvant therapy, only 4–12% of cases achieve this outcome [6]. Major pathological response (MPR), another key indicator, has been closely linked to overall survival (OS) in NSCLC patients [7]. Additionally, peripheral blood markers and imaging techniques have provided valuable prognostic insights, especially in patients undergoing immunotherapy [8]. Computed tomography (CT) and positron emission tomography (PET-CT) have proven to be highly accurate diagnostic tools for disease assessment, contributing to improved clinical decision making [9, 10].

While previous studies have attempted to identify clinical factors that can predict pathological response in resectable NSCLC patients [11], a consensus on the most predictive factors has yet to be reached [12]. Thus, the primary aim of this study was to evaluate clinical factors, derived from non-invasive methods, that could predict pathological response in NSCLC patients, ultimately contributing to the development of personalized treatment strategies.

Materials and Methods

Cases

From June 2018 to January 2023, a total of 212 patients with resectable NSCLC (stages IB-IIIA) who received neoadjuvant chemotherapy combined with immune checkpoint inhibitors (ICIs) were enrolled at institution 1. An additional 85 patients from three other centers were included in the study, and the distribution of these multicenter cases is detailed in Supplementary Table S1. All patients underwent radical surgery following their treatment.

The inclusion criteria were: (1) Patients had stage IB to stage IIIA resectable NSCLC demonstrated histologically or cytologically; (2) PET-CT performed both before treatment and prior to surgery, the time interval for PET-CT scanning after neoadjuvant immunotherapy is recommended to be evaluated every 2 cycles during the treatment cycle, with a final evaluation 4–6 weeks after the end of the last treatment; (3) administration of at least four cycles of neoadjuvant chemotherapy in combination with ICIs

(nivolumab, pembrolizumab, sindilizumab, camrelizumab, or tislelizumab) preoperatively; (4) peripheral blood indicators were assessed at both baseline and pre-surgery; (5) patients underwent surgery following neoadjuvant therapy; (6) all surgeries resulted in R0 resections, indicating that no residual tumor tissue was observed microscopically; (7) systematic lymph node dissection was performed for all patients, with the number of lymph nodes dissected being quality-controlled to ensure the accuracy of N-staging.

The exclusion criteria were: (1) patients who had received any form of treatment prior to the initial diagnosis at our center or the other three centers; (2) patients unwilling to complete the treatment prior to surgery; (3) patients with benign tumors.

Clinical factors collection and treatment

Baseline (B) and preoperative (P) CT/PET-CT scans were collected by attending clinicians. Peripheral blood markers, including hemoglobin (HGB), white blood cell count (WBC), absolute neutrophil count (NEC), lymphocyte count (LYM), monocyte count (MON), platelet count (PLT), and lactate dehydrogenase (LDH), were measured. Tumor markers, such as total prostate-specific antigen (TPSA), squamous cell carcinoma antigen (SCC), gastrin-releasing peptide precursor (ProGRP), neuron-specific enolase (NSE), carbohydrate antigen 199 (CA199), carcinoembryonic antigen (CEA), and cytokeratin fragment antigen (Cyfra), were also analyzed. Neutrophil-to-lymphocyte ratio (NLR), platelet-to-lymphocyte ratio (PLR), and lymphocyte-to-monocyte ratio (LMR) were then calculated. Additional factors, such as alanine aminotransferase (ALT), alkaline phosphatase (ALP), total bilirubin (TBIL), and creatinine (Cr), were monitored to assess potential immunotherapy-related adverse effects.

Demographic and clinical data, including gender, age, tumor location, tumor size, pathological type, stage, and response, were collected. Tumor stage and pathological classification were based on the ninth edition of the TNM classification. All clinical data were obtained from the Department of Lung Cancer Surgery across participating centers. The Mann–Whitney U test was used to assess significant differences between continuous variables in the training (TRA) and testing (TES) cohorts. Normality of continuous variables was evaluated using quantile–quantile plots (Supplementary Fig. S1 and Supplementary Table S2) to ensure the appropriateness of statistical tests.

Study assessment

Patients were instructed to fast for at least 6 h before the scan. Blood glucose levels were maintained below 140 mg/dl to ensure optimal Fluorine-18 FluoroDeoxyGlucose (18F-FDG) uptake. Each patient received an intravenous injection of 3.7–7.4 MBq/kg (0.1–0.2 mCi/kg) of 18F-FDG, followed by a 60-min rest period for optimal uptake prior to scanning.

The tumor target volume was defined using PET VCAR software (GE Healthcare, USA) on the GE Advantage Workstation 4.6 (AW 4.6) by applying an isocontour threshold of 41% of the maximum SUV (SUV_{max}). All PET/CT images were independently contoured by three experienced radiologists, with discrepancies resolved through consensus to ensure accuracy. SUVmax was automatically calculated within the tumor target volume. The details of the parameters described above are shown in Supplementary Table S3.

A patient was deemed to have achieved pCR when no residual cancer cells were present in the tissue or lymph nodes. MPR was defined as a reduction in the area of cancer cells to less than 10%. Clinical stage, downstaging, and therapy efficiency were evaluated prior to surgical intervention. The Response Evaluation Criteria in Solid Tumors (RECIST, version 1.1) was employed to analyze the changes observed in the CT/PET-CT scans. Furthermore, changes in the maximum standard uptake value (SUV_{max}) of both tumors and lymph nodes were recorded after PET scan. In cases where mediastinal lymph node metastasis was suspected prior to surgery, biopsies were performed. In accordance with the RECIST assessment, the clinical response was classified into four categories: complete response (CR), partial and minor response (PR), stable disease (SD), and progressive disease (PD).

Statistical analysis

All statistical analyses were performed using R software (version 4.3.1). Categorical variables were evaluated using Chi-squared and Fisher's exact tests, with results expressed as percentages. Continuous variables were analyzed with Student's t test and reported as mean ± standard deviation. These methods were used to compare baseline clinical characteristics between the TRA and TES. A tenfold LASSO regression analysis was used to identify key prognostic features, focusing on binary outcome variables such as pCR and MPR, given their dichotomous and non-time-dependent nature. Logistic regression was subsequently applied to these binary outcomes, with LASSO used for variable selection. The cases were classified into high-risk (HI) and low-risk (LO) groups based on 75 clinical indicators, as determined by tenfold LASSO selection. The thresholds for the HI and LO groups were determined based on the results of the logistic regression analysis.

The calibrate function, combined with bootstrapping, was employed to generate calibration plots, which were

further analyzed using linear regression to calculate the calibration slope and intercept. A summary of the intercept and slope values from the calibration analysis is available in Supplementary Table S4.

Results

Patient characteristics

A total of 212 and 85 cases were allocated to the TRA and TES sets, respectively. The baseline characteristics of each case are provided in Table 1 for comparison. The study workflow is illustrated in Fig. 1. The cases were classified into HI and LO groups based on 75 clinical indicators, as determined by tenfold LASSO selection. All variables were selected through LASSO analysis and logistic regression, using variables cross-validated by the tenfold LASSO method (Supplementary Fig. S2).

pCR prediction in TRA and TES sets coefficient

The protective factors' coefficients for achieving pCR included the change in tumor SUV_{max} (delta-Tumor-SUV_{max}), tumor area, and RAS mutation, while the hazard factors' coefficients included preoperative tumor SUV_{max} (P-tumor-SUV_{max}), preoperative maximum tumor diameter (P-Tumor-max), and baseline neutrophil count (B-NEC) (Fig. 2A). The coefficients used for pCR prediction are provided in Table 2. The corresponding nomogram for pCR prediction was illustrated (Fig. 2B). The area under the curve (AUC) for pCR prediction was 0.97 in TRA and 0.88 in TES (Fig. 2C, D). The accuracy for predicting pCR was 89.2% in TRA and 87.1% in TES (Supplementary Table S5).

MPR prediction in TRA and TES sets coefficient

The protective factors' coefficients for achieving MPR were delta-Tumor-SUV_{max}, B-P-tumor reduction, and P-ALT, while the hazard factors' coefficients were P-tumor-SUV_{max} and B-TPSA (Fig. 3A). The corresponding nomogram for MPR prediction is illustrated (Fig. 3B). The coefficients used in the MPR prediction model are provided in Table 2. And the AUC for MPR prediction was 0.98 in TRA and 0.81 in TES (Fig. 3C, D).

Delta-SUV_{max}-tumor demonstrated a strong protective effect in both pCR and MPR predictions, while P-tumor-SUV_{max} showed an opposite effect. The CT/PET-CT values demonstrated a strong capacity to predict the pathological response. The accuracy for predicting MPR was 90.6% in TRA and 70.6% in TES (Supplementary Table S5). These findings suggest that the model has significant predictive value for pathological response as illustrated by the nomogram.

The prediction nomogram for MPR was developed using the three factors that demonstrated the strongest predictive power during the model-building process. While P-ALT and B-TPSA were included in the initial set of 75 clinical indicators, they were not selected as top predictors for MPR based on the results of our tenfold LASSO selection. The final selection of factors was based on their statistical significance and their ability to contribute to the model's predictive accuracy.

Evaluation of the model for predicting pCR and MPR

The DCA demonstrated that all nomograms provided clinical benefit in predicting pCR and MPR (Fig. 4A, B) in the TRA and TES sets across a broad range of threshold probabilities. The calibration curves demonstrated a high level of concordance between the nomogram's predictions and actual pCR data in the TRA and TES sets (Fig. 4C, D). Similarly, MPR predictions were comparable between the TRA and TES sets (Fig. 4E, F). Additionally, adding clinical factors improves the single imaging model's performance, with results in Supplementary Table S6. The combined model demonstrates higher AUC values.

Discussion

Our main finding was that imaging indicators combined with other clinical indicators perform good predictive power for pathological remission in patients with neoadjuvant immunotherapy combined with chemotherapy. Similar to our findings, higher baseline levels of certain blood factors have been identified as independent predictors of outcomes in NSCLC patients with local metastasis receiving immunotherapy [13]. Blood factors such as neutrophil-to-lymphocyte ratio (NLR) and lactate dehydrogenase (LDH) have been associated with improved outcomes [14]. However, in our study, no significant differences in these factors were observed across different patient groups. The prognostic and predictive utility of CT/PET-CT imaging in lung cancer has been extensively studied [15], and the predictive value of age in various tumors is well-established. Moreover, the accuracy of imaging data in predicting pathological response has been supported by previous research [16]. In our analysis, the accuracy for predicting pathological response was 89.2% in TRA and 87.1% in TES, demonstrating the feasibility of precise prediction for pCR in NSCLC patients treated with neoadjuvant chemotherapy combined with immunotherapy.

Table 1 Clinical characteristics of the cases in this study

Characteristics	Training set $n=212$	Testing set $n=85$	*P* value	Characteristics	Training set $n=212$	Testing set $n=85$	*P* value
Age (mean (SD))	61.25 (7.23)	59.92 (7.66)	0.161	P-N Stage (%)	–	–	0.141
Gender—male (%)	172 (81.1)	65 (76.5)	0.457	N0	142 (67.0)	50 (58.8)	
Imm cycle (mean (SD))	2.21 (0.85)	1.33 (0.47)	< 0.001	N1	16 (7.5)	4 (4.7)	
Tumor area (%)	–	–	< 0.001	N2	54 (25.5)	31 (36.5)	
LLL	39 (18.4)	18 (21.2)		Lobectomy	196 (92.45)	80 (94.12)	0.803
LUL	47 (22.2)	27 (31.8)		Pneumonectomy	16 (7.55)	5 (5.78)	
RUL	43 (20.3)	18 (21.2)		B-TNM stage (%)	–	–	0.249
RML	12 (5.7)	22 (25.9)		IB	26 (12.3)	7 (8.2)	
RLL	71 (33.5)	0 (0.0)		II	42 (19.8)	12 (14.1)	
Smoking (%)	184 (86.8)	52 (61.2)	< 0.001	III	144 (67.9)	66 (77.6)	
Pathology (%)	–	–	< 0.001	P-TNM stage (%)	–	–	0.021
Adenocarcinoma	56 (26.4)	33 (38.8)		IB	83 (39.2)	43 (50.6)	
Lepidic type	11 (5.3)	7 (8.2)		II	68 (32.1)	13 (15.3)	
Acinar type	10 (4.7)	6 (7.1)		III	59 (27.8)	29 (34.1)	
Papillary type	10 (4.7)	8 (9.4)		T0N0M0	2 (0.9)	0 (0.0)	
Micropapillary type	9 (4.2)	4 (4.7)		B-Tumor-max (mean (SD))	4.89 (2.00)	4.96 (1.30)	0.76
Solid type	16 (7.5)	8 (9.4)		P-Tumor-max (mean (SD))	3.20 (1.89)	2.65 (1.08)	0.012
Squamous carcinoma	142 (67.0)	52 (61.2)	< 0.001	B-lymph-short (mean (SD))	1.21 (1.71)	1.71 (0.31)	0.008
Keratinizing squamous cell lung carcinoma	78 (36.8)	32 (37.6)		P-lymph-short (mean (SD))	0.88 (0.50)	1.22 (0.43)	< 0.001
Non-keratinizing squamous cell lung carcinoma	64 (30.2)	20 (23.6)		B-P-tumor reduction (mean (SD))	1.68 (1.60)	2.13 (1.58)	0.03
Others	14 (6.6)	0 (0.0)	< 0.001	B-P-tumor reduction percentage (mean (SD))	0.34 (0.29)	0.44 (0.23)	0.004
Large cell carcinoma	5 (2.4)	0 (0.0)		B-P-lymph-reduction (mean (SD))	0.33 (1.68)	0.48 (0.53)	0.422
Adenosquamous carcinoma	9 (4.2)	0 (0.0)		B-P-lymph-reduction (mean (SD))	0.16 (0.41)	0.23 (0.41)	0.153
Location (%)	124 (58.5)	48 (56.5)	0.85	EGFR wild type (%)	209 (98.6)	84 (98.8)	1
Chemotherapy (%)	–	–	< 0.001	ALK positive (%)	9 (4.2)	3 (3.5)	1
PC	7 (3.3)	31 (36.5)		ROS1 negative (%)	207 (97.6)	80 (94.1)	0.244
PP	51 (24.1)	1 (1.2)		RAS negative (%)	204 (96.2)	80 (94.1)	0.625
TC	31 (14.6)	53 (62.4)		B-TPSA (mean (SD))	140.39 (158.91)	137.03 (40.27)	0.848
TP	123 (58.0)	0 (0.0)		P-TPSA (mean (SD))	82.31 (137.51)	71.84 (10.24)	0.484
Antibody (%)			< 0.001	B-SCC (mean (SD))	2.47 (3.57)	1.69 (1.41)	0.051
Atezolizumab	75 (35.4)	46 (54.1)		P-SCC (mean (SD))	1.63 (2.16)	1.19 (0.99)	0.069
Camrelizumab	11 (5.2)	39 (45.9)		B-ProGRP (mean (SD))	40.31 (40.69)	40.35 (8.52)	0.993
Nivolumab	25 (11.8)	0 (0.0)		P-ProGRP (mean (SD))	35.35 (10.01)	38.32 (6.91)	0.013
Pembrolizumab	41 (19.3)	0 (0.0)		B-NSE (mean (SD))	17.47 (6.67)	19.84 (3.07)	0.002
Sindilizumab	47 (22.2)	0 (0.0)		P-NSE (mean (SD))	13.77 (3.15)	12.46 (2.12)	< 0.001
Tislelizumab	13 (6.1)	0 (0.0)		B-CA199 (mean (SD))	18.47 (26.15)	21.80 (3.43)	0.242
Clinical evaluation (%)	–	–	< 0.001	P-CA199 (mean (SD))	17.09 (24.44)	14.58 (5.77)	0.349
CR	12 (5.7)	59 (69.4)		B-CEA (mean (SD))	15.39 (35.65)	8.99 (1.77)	0.099
PD	2 (0.9)	26 (30.6)		P-CEA (mean (SD))	6.95 (32.38)	5.13 (1.56)	0.605
PR	131 (61.8)	0 (0.0)		B-Cyfra (mean (SD))	9.30 (15.41)	9.39 (1.82)	0.955
SD	67 (31.6)	0 (0.0)		P-Cyfra (mean (SD))	3.92 (6.68)	3.16 (1.79)	0.306
B-Tumor-SUV_{max} (mean (SD))	16.47 (5.91)	17.94 (5.90)	0.052	B-HGB (mean (SD))	140.64 (21.02)	146.29 (15.12)	0.025
P-Tumor-SUV_{max} (mean (SD))	8.44 (5.53)	9.53 (5.63)	0.131	P-HGB (mean (SD))	124.03 (17.61)	129.87 (16.27)	0.009

Table 1 (continued)

Characteristics	Training set $n=212$	Testing set $n=85$	*P* value	Characteristics	Training set $n=212$	Testing set $n=85$	*P* value
Delta-SUV_{max} -Tumor (mean (SD))	8.02 (6.15)	8.42 (6.53)	0.623	B-WBC (mean (SD))	7.49 (2.13)	6.84 (1.04)	0.008
B-Lymph-SUV_{max} (mean (SD))	5.29 (3.80)	5.85 (3.98)	0.252	P-WBC (mean (SD))	6.06 (1.80)	6.67 (1.30)	0.005
P-Lymph-SUV_{max} (mean (SD))	2.37 (2.20)	2.61 (2.20)	0.398	B-NEC (mean (SD))	4.77 (1.76)	4.83 (1.27)	0.76
Delta-SUV_{max} -Lymph (mean (SD))	2.92 (3.62)	3.13 (3.59)	0.64	P-NEC (mean (SD))	3.47 (1.48)	3.65 (1.49)	0.345
T downstaging (%)	120 (56.6)	45 (52.9)	0.656	B-PLT (mean (SD))	267.78 (82.42)	246.05 (50.21)	0.024
N downstaging (%)	98 (46.2)	41 (48.2)	0.853	P-PLT (mean (SD))	221.23 (74.52)	213.45 (62.57)	0.397
TNM downstaging (%)	114 (53.8)	48 (56.5)	0.77	B-LYM (mean (SD))	1.95 (0.61)	2.01 (0.65)	0.475
B-T stage (%)	–	–	< 0.001	P-LYM (mean (SD))	1.80 (0.56)	1.78 (0.56)	0.804
T1	41 (19.3)	4 (4.7)		B-NLR (mean (SD))	4.10 (1.42)	3.77 (1.31)	0.067
T2	85 (40.1)	45 (52.9)		P-NLR (mean (SD))	3.60 (1.34)	4.18 (1.72)	0.002
T3	60 (28.3)	36 (42.4)		B-MON (mean (SD))	0.55 (0.21)	0.78 (0.21)	< 0.001
T4	26 (12.3)	0 (0.0)		P-MON (mean (SD))	0.57 (0.19)	0.60 (0.17)	0.22
B-N stage (%)	–	–	< 0.001	B-ALT (mean (SD))	20.15 (13.97)	22.33 (5.05)	0.161
N0	67 (31.6)	5 (5.9)		P-ALT (mean (SD))	21.45 (13.70)	21.99 (6.86)	0.728
N1	8 (3.8)	17 (20.0)		B-ALP (mean (SD))	92.14 (27.33)	98.35 (11.97)	0.044
N2	137 (64.6)	63 (74.1)		P-ALP (mean (SD))	84.71 (24.38)	114.59 (24.02)	< 0.001
P–T stage (%)	–	–	< 0.001	B-TBIL (mean (SD))	11.67 (6.18)	12.52 (2.06)	0.215
T0	3 (1.4)	60 (70.6)		P-TBIL (mean (SD))	9.59 (3.94)	11.20 (2.82)	0.001
T1	107 (50.5)	19 (22.4)		B-Cr (mean (SD))	71.98 (12.87)	75.50 (17.26)	0.055
T2	72 (34.0)	6 (7.1)		P-Cr (mean (SD))	76.39 (15.27)	78.30 (21.21)	0.387
T3	25 (11.8)	0 (0.0)		B-UREA (mean (SD))	6.67 (19.80)	5.09 (1.15)	0.464
T4	5 (2.4)	0 (0.0)		P-UREA (mean (SD))	5.93 (1.48)	5.72 (1.34)	0.256
				B-LDH (mean (SD))	195.38 (48.09)	191.01 (23.11)	0.424
				P-LDH (mean (SD))	202.88 (43.30)	207.72 (26.23)	0.337

ALK: anaplastic lymphoma kinase; ALP: alkaline phosphatase; ALT: alanine aminotransferase; B: baseline; CA199: carbohydrate antigen199; CEA: carcinoembryonic antigen; Cr: creatinine; CR: complete response; Cyfra: cytokeratin fragment antigen; EGFR: estimated glomerular filtration rate; HGB: hemoglobin; Imm: immunotherapy; LDH: lactate dehydrogenase; LLL: left lower lobe; LMR: lymphocyte-to-monocyte ratio; LUL: left upper lobe; LYM: absolute lymphocyte count; Lymph: Lymph nodes; M: metastasis; MON: absolute monocyte count; N: node; NEC: absolute neutrophil count; NLR: neutrophil-to-lymphocyte ratio; NSE: neuron-specific enolase; P: preoperative; pCR: pathological complete response; PC: pemetrexed and carboplatin; PD: progressing disease; PLR: platelet-to-lymphocyte ratio; PLT: platelet; PP: pemetrexed and cisplatin; ProGRP: gastrin-releasing peptide precursor; pTNM stage: pathological TNM stage; RLL: right lower lobe; RML: right middle lobe; ROS1: c-ros oncogene 1 kinase; PR: partial response; RUL: right upper lobe; SCC: squamous cell carcinoma antigen; SD: stable disease; SUV_{max}: standard uptake value; T: tumor; TBIL: total bilirubin; TC: paclitaxel and cisplatin TNM: tumor-node metastasis; TP: paclitaxel, cisplatin; TPSA: total prostate-specific antigen; UREA: urea nitrogen; WBC: white blood cells

These results are consistent with findings from clinical trials investigating the efficacy of neoadjuvant chemotherapy [17]. Notably, the predictive model developed in this study demonstrates superior capability for predicting both pCR and MPR compared to models based solely on CT or PET-CT [18, 19]. Predictive models incorporating multiple factors are believed to achieve higher accuracy. This is because neoadjuvant therapy can alter tumor morphology, making pCR prediction more challenging [20]. A previous study using radiomics data to predict response, with AUCs ranging from 0.76 to 0.80 [21]. Similarly, our model combined with clinical factors showed high sensitivity for MPR prediction, including in TNM downstaging as well as lesion and lymph node size reduction. Notably, the prediction of both T downstaging and N downstaging proved to be valuable for overall survival (OS) comparison [22].

Our model's strengths include simplicity, clinical practicality, and superior interpretability. Unlike tumor mutation burden and microsatellite instability [23], our model uses routine clinical assessments, making it more accessible and cost-effective. Additionally, it surpasses radiomics in clarity, enabling easier clinical application

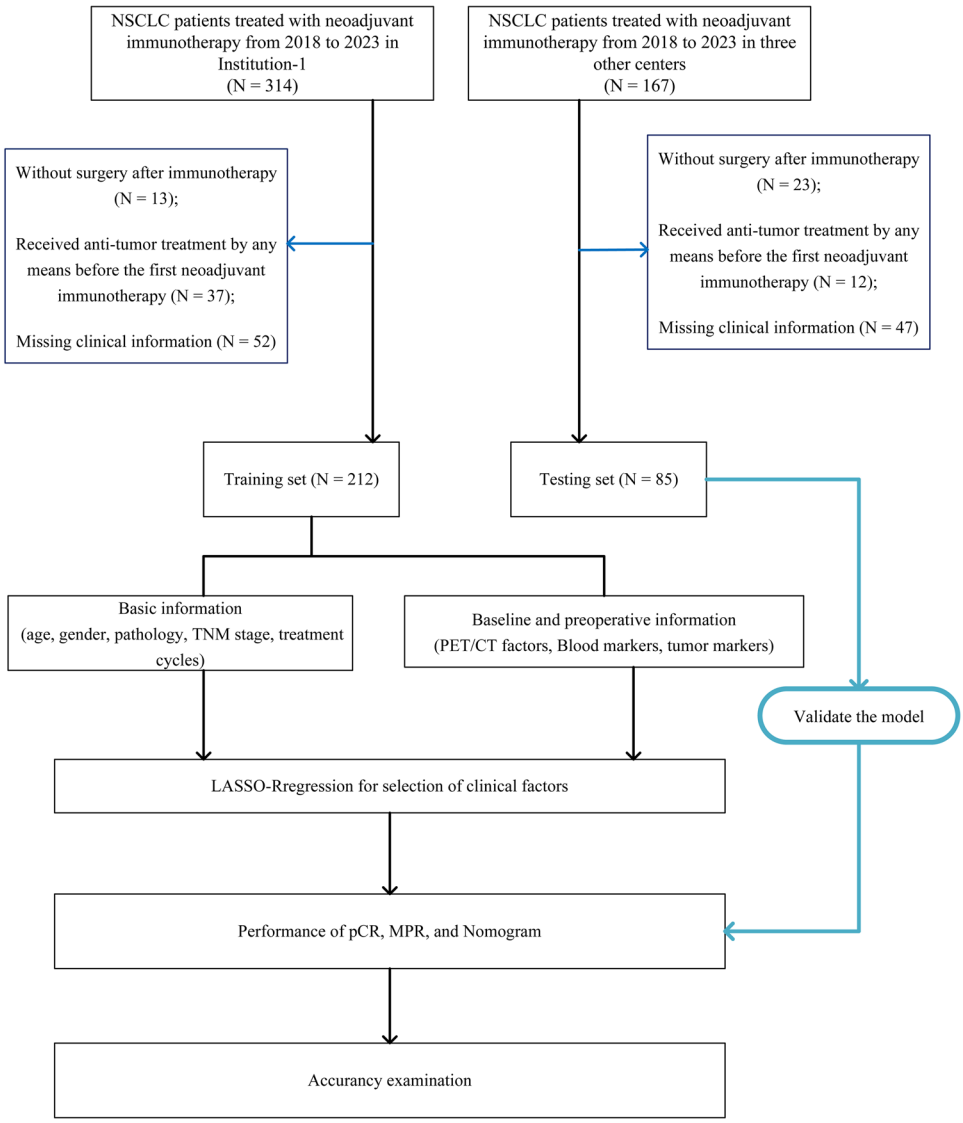

Fig. 1 The flow chart shows the outline of the research. NSCLC: non-small cell lung cancer; pCR: pathological complete response; MPR: major pathological response; DCA: decision curve analysis

[24]. Our model's robust performance on external datasets demonstrates its generalizability, crucial for clinical utility. This consistency across datasets underscores its reliability and makes it a valuable tool for predicting neoadjuvant immunotherapy responses in lung cancer patients.

The utility of imaging in predicting response to neoadjuvant PD-1 blockade in NSCLC patients has been previously demonstrated [25]. Similarly, Cottrell et al. found that CT imaging is a useful tool for evaluating clinical response [26]. In our study, P-Tumor-SUV_{max} and delta-Tumor-SUV_{max} were identified as robust predictors, further supporting the combined use of imaging and pathology for evaluating disease progression. However, the debate regarding whether preoperative CT imaging can accurately predict postoperative prognosis remains unresolved [27]. Imaging factors obtained from CT or PET do not directly assess tumor response to treatment. Nonetheless, changes in SUV_{max} in tumors and lymph nodes can indicate alterations in tumor cell metabolism, which may reflect treatment response [28].

Changes in SUVmax reflect changes in tumor cell metabolic activity; studies have shown that changes in SUVmax are related to tumor cell proliferation, hypoxia, and patient outcomes [29]. In some studies, baseline SUVmax is related to tumor cell proliferation and patient prognosis, indicating that SUVmax can be used as a tool to assess tumor metabolic activity and prognosis [30]. The outperform of total lesion glycolysis (TLG) and metabolic tumor volume (MTV) in predicting histopathologic response has been proved [31]; they combined the metabolic activity of the tumor with regional indicators for a systematic assessment of the disease and highlighted the use of PET-CT [32]. Although TLG and MTV own the advantages described above, the SUVmax was chosen for its widespread use, reproducibility, and

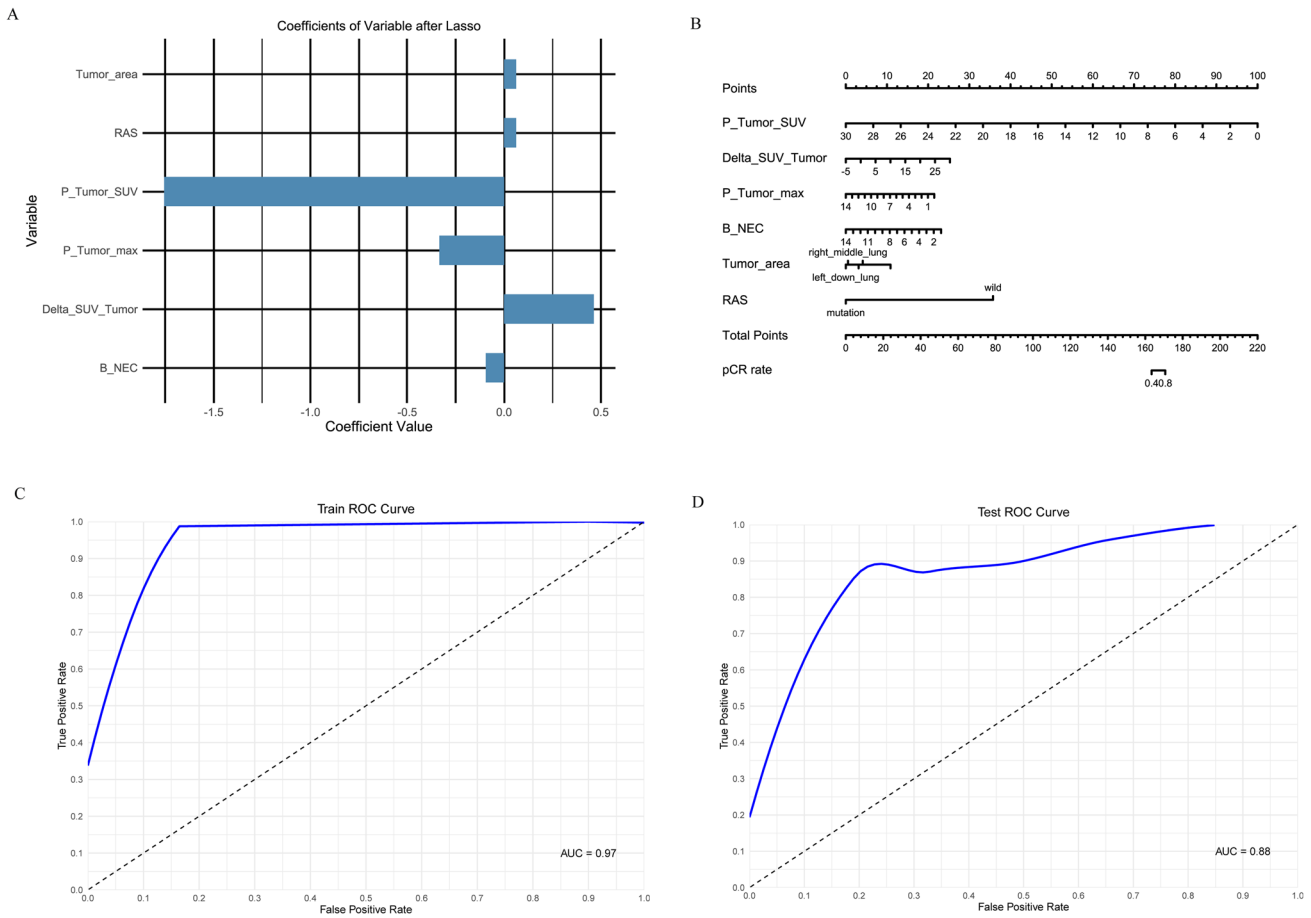

Fig. 2 Screening the candidate variables for predicting pathological complete response. Coefficients of variable for pCR after LASSO **A**. Nomogram for reaching pCR **B**. Receiver operating characteristic curve (ROC) for pCR prediction in training set **C**, ROC curve for pCR prediction in testing set **D**. Abbreviations: baseline, B; preoperative, P

Table 2 Coefficients value of the predictive factors in the model

Items for coefficients	Coefficients value	
pCR prediction	Delta-Tumor-SUV_{max}	0.464
	Tumor area	0.062
	RAS-positive	0.062
	P-tumor-SUVmax	− 1.756
	P-tumor-diameter-maximum	− 0.334
	B-NEC	− 0.094
MPR prediction	Delta-Tumor-SUVmax	0.695
	B-P-tumor reduction	0.195
	P-ALT	0.011
	P-tumor-SUVmax	− 1.901
	B-TPSA	− 0.018

Abbreviations: ALT: alanine aminotransferase; MPR: major pathological response; NEC: absolute neutrophil count; pCR: pathological complete response; RAS: RAS-driven gene mutation; SUV_{max}, maximum standard uptake value; TPSA: total prostate-specific antigen

ability to reflect tumor metabolic activity. It is less sensitive to contouring variations compared to MTV and TLG, making it more reliable for multicenter studies. And that is the reason we chose SUVmax as the model's marker.

Thus, it is suggested that clinical factors are combined in a more systematic approach to create a superior predictive model for patient outcomes. In our study, the overall change delta-Tumor-SUV_{max} was greater in the LO group compared to the HI group, which is in agreement with a previous report [33]. Our previous study has shown the ability to predict survival in NSCLC [34]; furthermore, we also demonstrated high accuracy in predicting both pCR and MPR.

In lung cancer, tumor markers are more commonly used to help diagnose, monitor treatment, and detect recurrence of lung cancer [35]. Although the prediction ability of PSA was relative weak compared with other factors in our model, it still owned the its value. Similarly, some researchers highlighted the value for PSA in non-prostrate cancer; tumor markers in circulating blood of lung cancer patients could indicate prognosis in lung cancer [36]. In real world,

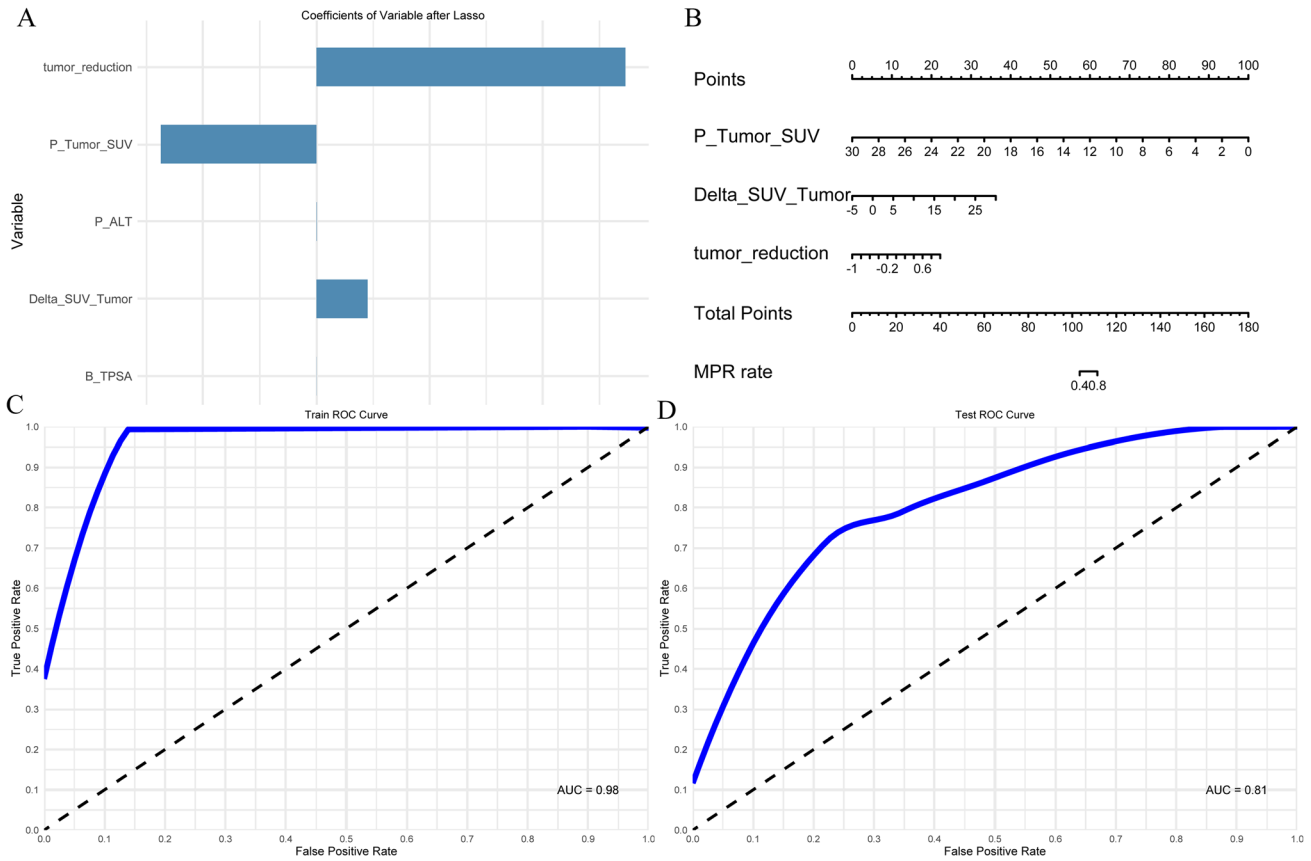

Fig. 3 Screening the candidate variables for predicting major pathological response. Coefficients of variable for MPR after LASSO **A**. Nomogram for reaching MPR **B**. Receiver operating characteristic curve (ROC) for MPR prediction in training set **C**, ROC curve for MPR prediction in testing set **D**. Abbreviations: baseline, B; preoperative, P

we supposed that the predictive power of PSA needs to be verified in subsequent multi-center studies to confirm this conclusion.

Despite these promising results, several limitations must be acknowledged. The data were obtained from NSCLC patients receiving neoadjuvant chemotherapy combined with ICIs, and other potential contributing factors, such as lifestyle and socioeconomic indicators, were not considered in our screening process. Additionally, our study's primary limitation is the small sample size, which may impact generalizability. Despite data from multiple centers, the limited number of cases could introduce variability and reduce model robustness. We addressed potential overfitting through cross-validation. Future research should include a larger patient population and extend the follow-up period to better evaluate long-term outcomes and refine the predictive models. Expanding the multicenter dataset will further validate the robustness of the model. Another limitation is the limited inclusion of molecular markers. The primary reason for including only a few molecular markers is their clinical accessibility and feasibility. Many potential biomarkers, while theoretically valuable, are not readily available in clinical practice due to technical limitations, high costs, or lack of standardized protocols for their measurement. Our goal was to focus on markers that are currently feasible for routine clinical use, ensuring that our findings could be directly applicable and actionable in a real-world setting. Incorporating additional biomarkers and imaging features as they become standardized will enhance predictive power and clinical applicability.

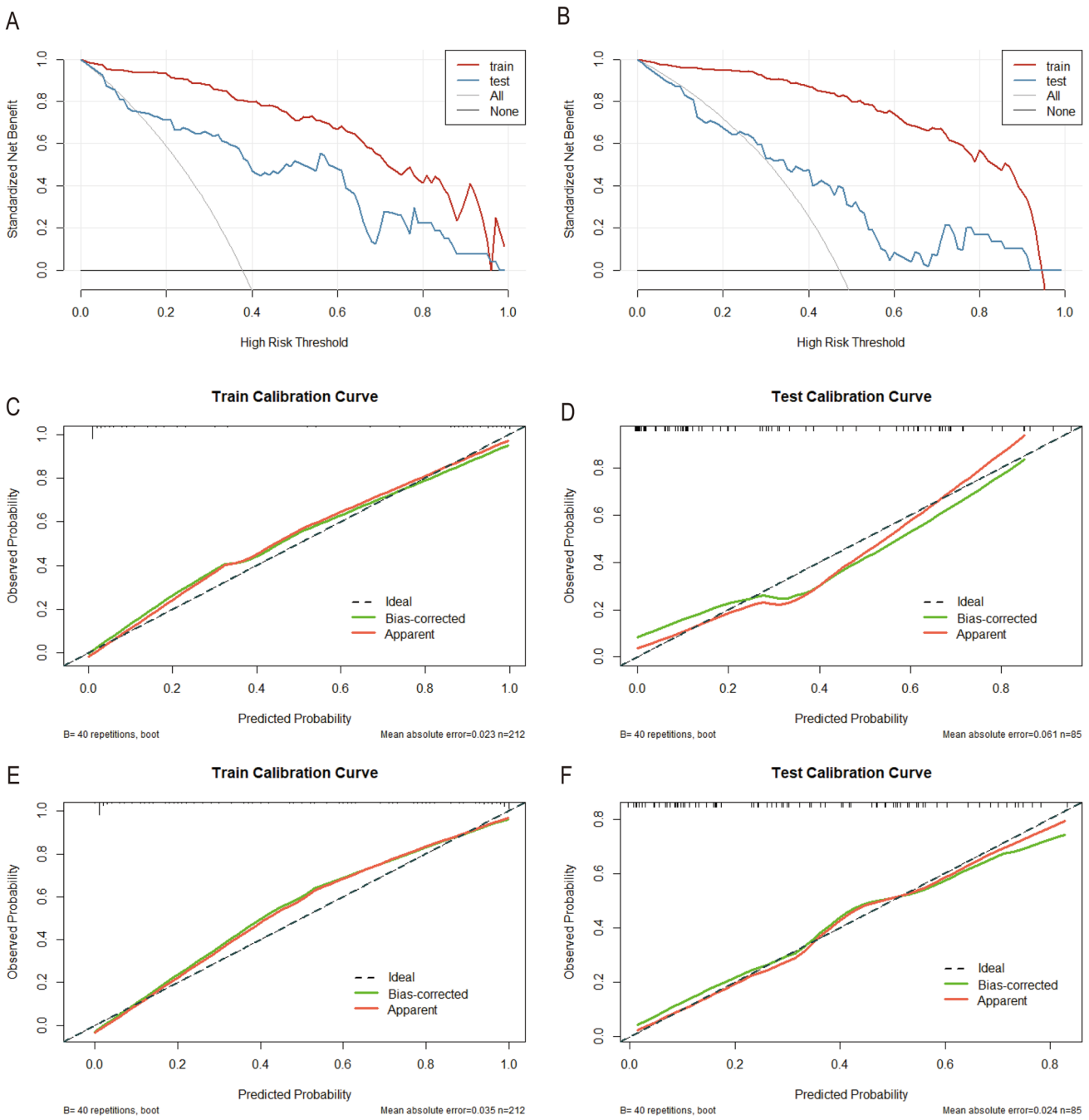

Fig. 4 Accuracy and validation of the model. DCA curve in pCR prediction **A** and MPR prediction **B**, the calibration curve in pCR training set **C**, pCR testing set **D**, MPR training set **E**, MPR testing set **F**. Abbreviation: pCR, pathological complete response; MPR, major pathological response

Conclusions

This multicenter study demonstrated that non-invasive tumor imaging and hematology can predict pathological response in NSCLC patients receiving neoadjuvant chemotherapy combined with ICIs. Preoperative tumor diameter, tumor SUV_{max}, changes in SUV_{max}, and tumor markers were particularly valuable for predicting pCR and MPR. These findings suggest that clinicians should consider these factors when personalizing treatment strategies for patients across multiple clinical settings.

Supplementary Information The online version contains supplementary material available at https://doi.org/10.1007/s00262-025-04017-z.

Author contributions All authors conducted the concept of the paper; all authors did the analysis and constructed the outline of the study. Zhenfa Zhang, Mengzhe Zhang, Meng Yan, and Pengpeng Zhang wrote the main manuscript text; Zekun Li, Zuo Liu, and Shuai Jiang prepared all the figures; Zekun Li prepared tables and figures; all authors reviewed the manuscript.

Funding There is no funding in our study.

Data availability No datasets were generated or analyzed during the current study.

Declarations

Competing interests The authors declare no competing interests.

Ethical approval and consent to participate This research was approved by the Ethics Committee of Tianjin Medical University Cancer Institute and Hospital, National Clinical Research Center for Cancer (Approval number: bc2022232). Our study followed the principles established in the Declaration of Helsinki, and all patients gave informed consent to participate.

References

1. Rami-Porta R et al (2024) The international association for the study of lung cancer lung cancer staging project: proposals for revision of the TNM stage groups in the forthcoming (Ninth) edition of the TNM classification for lung cancer. J Thorac Oncol 19:1007–1027. https://doi.org/10.1016/j.jtho.2024.02.011
2. Sidaway P (2024) From ESMO 2023: advances in lung cancer. Nat Rev Clin Oncol 21:4. https://doi.org/10.1038/s41571-023-00838-y
3. Hirsch FR et al (2017) Lung cancer: current therapies and new targeted treatments. Lancet 389:299–311. https://doi.org/10.1016/S0140-6736(16)30958-8
4. Jeong H et al (2024) Epithelial-mesenchymal transition induced by tumor cell-intrinsic PD-L1 signaling predicts a poor response to immune checkpoint inhibitors in PD-L1-high lung cancer. Br J Cancer 131:23–36. https://doi.org/10.1038/s41416-024-02698-4
5. Thompson JC et al (2020) Gene signatures of tumor inflammation and epithelial-to-mesenchymal transition (EMT) predict responses to immune checkpoint blockade in lung cancer with high accuracy. Lung Cancer 139:1–8. https://doi.org/10.1016/j.lungcan.2019.10.012
6. Liu S-Y et al (2023) Neoadjuvant nivolumab with or without platinum-doublet chemotherapy based on PD-L1 expression in resectable NSCLC (CTONG1804): a multicenter open-label phase II study. Signal Transduct Target Ther 8:442. https://doi.org/10.1038/s41392-023-01700-4
7. Dacic S et al (2023) International association for the study of lung cancer study of reproducibility in assessment of pathologic response in resected lung cancers after neoadjuvant therapy. J Thorac Oncol 18:1290–1302. https://doi.org/10.1016/j.jtho.2023.07.017
8. Palermo B et al (2023) CD28/PD1 co-expression: dual impact on CD8+ T cells in peripheral blood and tumor tissue, and its significance in NSCLC patients' survival and ICB response. J Exp Clin Cancer Res 42:287. https://doi.org/10.1186/s13046-023-02846-3
9. Deng J et al (2022) Lung cancer with PET/CT-defined occult nodal metastasis yields favourable prognosis and benefits from adjuvant therapy: a multicentre study. Eur J Nucl Med Mol Imaging 49:2414–2424. https://doi.org/10.1007/s00259-022-05690-3
10. Sujit SJ et al (2024) Enhancing NSCLC recurrence prediction with PET/CT habitat imaging, ctDNA, and integrative radiogenomics-blood insights. Nat Commun 15:3152. https://doi.org/10.1038/s41467-024-47512-0
11. Cheng Y, Chen Z-Y, Huang J-J, Shao D (2023) Efficacy evaluation of neoadjuvant immunotherapy plus chemotherapy for non-small-cell lung cancer: comparison of PET/CT with postoperative pathology. Eur Radiol 33:6625–6635. https://doi.org/10.1007/s00330-023-09922-4
12. Xu Y et al (2019) Deep learning predicts lung cancer treatment response from serial medical imaging. Clin Cancer Res 25:3266–3275. https://doi.org/10.1158/1078-0432.CCR-18-2495
13. Huang J et al (2024) The international association for the study of lung cancer staging project for lung cancer: proposals for the revision of the N descriptors in the forthcoming ninth edition of the TNM classification for lung cancer. J Thorac Oncol 19:766–785. https://doi.org/10.1016/j.jtho.2023.10.012
14. Diem S et al (2017) Neutrophil-to-lymphocyte ratio (NLR) and platelet-to-lymphocyte ratio (PLR) as prognostic markers in patients with non-small cell lung cancer (NSCLC) treated with nivolumab. Lung Cancer 111:176–181. https://doi.org/10.1016/j.lungcan.2017.07.024
15. Hicks RJ (2022) The value of the standardized uptake value (SUV) and metabolic tumor volume (MTV) in lung cancer. Semin Nucl Med 52:734–744. https://doi.org/10.1053/j.semnuclmed.2022.04.007
16. Buizza G et al (2018) Early tumor response prediction for lung cancer patients using novel longitudinal pattern features from sequential PET/CT image scans. Phys Med 54:21–29. https://doi.org/10.1016/j.ejmp.2018.09.003
17. Cascone T et al (2023) Neoadjuvant durvalumab alone or combined with novel immuno-oncology agents in resectable lung cancer: the phase II NeoCOAST platform trial. Cancer Discov 13:2394–2411. https://doi.org/10.1158/2159-8290.CD-23-0436
18. Yang M et al (2024) [18F]FDG PET-CT radiomics signature to predict pathological complete response to neoadjuvant chemo-immunotherapy in non-small cell lung cancer: a multicenter study. Eur Radiol 34:4352–4363. https://doi.org/10.1007/s00330-023-10503-8
19. Guo R et al (2024) The utility of 18F-FDG PET/CT for predicting the pathological response and prognosis to neoadjuvant immunochemotherapy in resectable non-small-cell lung cancer. Cancer Imaging 24:120. https://doi.org/10.1186/s40644-024-00772-x
20. She Y et al (2022) Deep learning for predicting major pathological response to neoadjuvant chemoimmunotherapy in non-small cell lung cancer: a multicentre study. EBioMedicine 86:104364. https://doi.org/10.1016/j.ebiom.2022.104364

21. Liao C-Y et al (2024) Personalized prediction of immunotherapy response in lung cancer patients using advanced radiomics and deep learning. Cancer Imaging 24:129. https://doi.org/10.1186/s40644-024-00779-4
22. Haro GJ et al (2019) Comparison of conventional TNM and novel TNMB staging systems for non-small cell lung cancer. JAMA Netw Open 2:e1917062. https://doi.org/10.1001/jamanetworkopen.2019.17062
23. Wang X et al (2024) Tumor mutational burden for the prediction of PD-(L)1 blockade efficacy in cancer: challenges and opportunities. Ann Oncol 35:508–522. https://doi.org/10.1016/j.annonc.2024.03.007
24. Prelaj A et al (2024) Artificial intelligence for predictive biomarker discovery in immuno-oncology: a systematic review. Ann Oncol 35:29–65. https://doi.org/10.1016/j.annonc.2023.10.125
25. Tao X et al (2020) The efficiency of 18F-FDG PET-CT for predicting the major pathologic response to the neoadjuvant PD-1 blockade in resectable non-small cell lung cancer. Eur J Nucl Med Mol Imaging 47:1209–1219. https://doi.org/10.1007/s00259-020-04711-3
26. Cottrell TR et al (2018) Pathologic features of response to neoadjuvant anti-PD-1 in resected non-small-cell lung carcinoma: a proposal for quantitative immune-related pathologic response criteria (irPRC). Ann Oncol 29:1853–1860. https://doi.org/10.1093/annonc/mdy218
27. Wu G et al (2021) Structural and functional radiomics for lung cancer. Eur J Nucl Med Mol Imaging 48:3961–3974. https://doi.org/10.1007/s00259-021-05242-1
28. Giesel FL et al (2021) FAPI-74 PET/CT using either 18F-AlF or Cold-Kit 68Ga labeling: biodistribution, radiation dosimetry, and tumor delineation in lung cancer patients. J Nucl Med 62:201–207. https://doi.org/10.2967/jnumed.120.245084
29. Rossi C et al (2022) Baseline SUVmax is related to tumor cell proliferation and patient outcome in follicular lymphoma. Haematologica 107:221–230. https://doi.org/10.3324/haematol.2020.263194
30. Xie Y et al (2021) A PET/CT nomogram incorporating SUVmax and CT radiomics for preoperative nodal staging in non-small cell lung cancer. Eur Radiol 31:6030–6038. https://doi.org/10.1007/s00330-020-07624-9
31. Burger IA et al (2016) 18F-FDG PET/CT of non-small cell lung carcinoma under neoadjuvant chemotherapy: background-based adaptive-volume metrics outperform TLG and MTV in predicting histopathologic response. J Nucl Med 57:849–854. https://doi.org/10.2967/jnumed.115.167684
32. Yamamoto S et al (2016) Radiogenomic analysis demonstrates associations between (18)F-fluoro-2-deoxyglucose PET, prognosis, and epithelial-mesenchymal transition in non-small cell lung cancer. Radiology 280:261–270. https://doi.org/10.1148/radiol.2016160259
33. Win T et al (2013) Tumor heterogeneity and permeability as measured on the CT component of PET/CT predict survival in patients with non-small cell lung cancer. Clin Cancer Res 19:3591–3599. https://doi.org/10.1158/1078-0432.CCR-12-1307
34. Zhang M et al (2024) Exploring clinical factors to predict the survival of patients with resectable non-small cell lung cancer with neoadjuvant immunotherapy. Eur J Cardiothorac Surg 66:335. https://doi.org/10.1093/ejcts/ezae335
35. Yu D, Du K, Liu T, Chen G (2013) Prognostic value of tumor markers, NSE, CA125 and SCC, in operable NSCLC patients. Int J Mol Sci 14:11145–11156. https://doi.org/10.3390/ijms140611145
36. Pérez-Ibave DC, Burciaga-Flores CH, Elizondo-Riojas M-Á (2018) Prostate-specific antigen (PSA) as a possible biomarker in non-prostatic cancer: a review. Cancer Epidemiol 54:48–55. https://doi.org/10.1016/j.canep.2018.03.009

Authors and Affiliations

Mengzhe Zhang[1] · Meng Yan[2] · Zekun Li[3] · Shuai Jiang[1] · Zuo Liu[1] · Pengpeng Zhang[1] · Zhenfa Zhang[1]

✉ Pengpeng Zhang
zpp19940120@tmu.edu.cn

✉ Zhenfa Zhang
zhangzhenfa@tmu.edu.cn

[1] Department of Lung Cancer Surgery, Tianjin Medical University Cancer Institute and Hospital, National Clinical Research Center for Cancer, Key Laboratory of Cancer Prevention and Therapy, Tianjin's Clinical Research Center for Cancer, Tianjin Lung Cancer Center, Tianjin 300060, China

[2] Department of Radiology, Tianjin Medical University Cancer Institute and Hospital, National Clinical Research Center for Cancer, Key Laboratory of Cancer Prevention and Therapy, Tianjin's Clinical Research Center for Cancer, Tianjin Lung Cancer Center, Tianjin 300060, China

[3] Department of Pancreatic Cancer, Tianjin Medical University Cancer Institute and Hospital, National Clinical Research Center for Cancer, Key Laboratory of Cancer Prevention and Therapy, Tianjin's Clinical Research Center for Cancer, Tianjin, China